Electrochemical Formation of Ca-Si in Molten $CaCl_2$-KCl

Y. Sakanaka,[a,z] T. Goto,[a] and Kan Hachiya[b]

[a]*Department of Science of Environment and Mathematical Modeling, Graduate School of Science and Engineering, Doshisha University, Kyoto, Japan*
[b]*Graduate School of Energy Science, Kyoto University, Kyoto, Japan*

Electrochemical formation of a Ca-Si film in a molten $CaCl_2$-KCl at 923 K was investigated. Potentiostatic electrolysis of a Si electrode at −0.10 V for 1 h resulted in the formation of a multiphase Ca-Si film having a thickness of about 30 μm. The Ca-Si film was converted into other alloy phases by anodic potentiostatic electrolysis after the cathodic electrodeposition of Ca metal at −0.10 V. The various transformation reactions and the corresponding equilibrium potentials were clarified. At 923 K, the equilibrium potential was found to be 0.18 V ($CaSi_2$). Reflectance measurements in the ultraviolet, visible, and near-infrared region clarified that the $CaSi_2$ film has a direct bandgap of 3.1 eV.
 [DOI: 10.1149/2.1021504jes]

Manuscript submitted December 11, 2014; revised manuscript received January 26, 2015. Published February 14, 2015.

Compound semiconductors are among the most promising materials for use in high-power electronic and photoelectric conversion devices because of their advantages.[1] However, conventional processes for preparing semiconductors involve high energy consumption and the use of hazardous starting materials, and are hence unsuitable for mass production. Therefore, a new semiconductor preparation process that does not require harmful starting materials or high energy has been proposed.

Recently, metal silicides, which are abundant, non-toxic materials, have attracted much interest for use as environment-friendly semiconductors, because they are expected to show excellent optical properties. In addition, the bandgap energy of metal silicides can be extended from the infrared to the visible region by appropriate choice of metal elements and phases of the compounds.[2–5]

Among the numerous metal silicides reported, Ca-Si metal silicides are well known semiconductor materials that exhibit superconductive properties. For example, Ca_2Si is a semiconductor with an energy gap of 1.9 eV,[6] while CaSi is expected to show high hydrogen storage capacity.[7] In addition, superconductivity has been discovered at 14 K under pressure in a new polymorph of the $CaSi_2$ stoichiometry.[8,9] Recently, there has been increased interest in the use of intermetallic silicides to replace the conventional graphite anodes in Li-ion batteries.[10,11] Films fabricated from these alloys, with arbitrary shapes and sizes, may be used in various applications such as energy conversion devices.

Nevertheless, the high vapor pressure of Ca makes the growth of a continuous film layer by deposition from the gas phase[12–17] difficult. Ca atoms are easily evaporated from the Si substrate, which prevents the formation of Ca-silicide by interdiffusion with the Si substrate.

With this background, we proposed a novel electrochemical process for the formation of silicide films. This process is advantageous because (1) the phases of the alloy films can be controlled by adjusting the electrochemical parameters and (2) the films can be grown on substrates of various shapes. We chose a calcium silicide as a model to confirm the feasibility of this process for producing silicide films, and investigated the electrodeposition of Ca and Si to form Ca-Si alloys in a molten $CaCl_2$-KCl system at 923 K.

Experimental

$CaCl_2$ (95.0%, Wako Pure Chemical Co. Ltd.) and KCl (99.5%, Wako Pure Chemical Co. Ltd.) were mixed in eutectic composition ($CaCl_2$:KCl = 38.4:61.6 mol%), and introduced in a high-purity alumina crucible (99.5 wt% Al_2O_3, SSA-S grade, NIKKATO Co. Ltd.), which was then kept under vacuum for more than 24 h at 473 K to ensure complete removal of water. All experiments were performed in the $CaCl_2$-KCl eutectic melt in a dry argon atmosphere. Temperature measurements were performed using a Chromel-Alumel thermocouple, with an accuracy of ±1 K. To investigate the electrochemical behavior, n-type Si plates (5 mm × 20 mm × 0.5 mm; 99.5%, Nilaco Co. Ltd.) were used as the working electrodes. The reference electrode was a silver wire immersed in $CaCl_2$-KCl containing 1 mol% of AgCl, placed in an alumina tube with a thin bottom to maintain electrical contact with the melt. The potential of the reference electrode was calibrated with reference to that of a M^{n+}/M electrode, which was prepared by electrodepositing an alkali metal on Mo wire. All potentials referred to in this paper are expressed with reference to the M^{n+}/M potential. The counter electrode was a glassy carbon rod (3 mm diameter; Tokai Carbon Co. Ltd.). A potentiostat/galvanostat (Hokuto Denko Co. Ltd. HZ-3000) was used for cyclic voltammetry and chronopotentiometry measurements. The samples were prepared by potentiostatic electrolysis and rinsed with ethylene glycol. The obtained samples were analyzed by X-ray diffractometry (XRD) with a Cu Kα line. The surface and cross-section of the samples were observed by scanning electron microscopy (SEM; JSM-7001, JEOL). For evaluation of the optical properties of the films, ultraviolet-visible-near infrared (UV-VIS-NIR) reflectance spectra were measured using a JASCO V-670 spectrophotometer.

Results and Discussion

Electrochemical window of $CaCl_2$-KCl.— Figure 1 shows the cyclic voltammograms obtained in $CaCl_2$-KCl at 923 K. A molybdenum wire and a glassy carbon rod were used as the working electrodes in the negative and positive potential regions, respectively. In the negative potential region, a sharp cathodic current and the corresponding anodic current were observed at about 0.10 V, which were attributable to the deposition of Ca or K metal and dissolution of the deposits, respectively. The current observed at a potential more negative than 0.4 V is due to the formation of Ca metal (activity smaller than 1) and its dissolution in $CaCl_2$. The potential at the cathodic limit was defined as the potential of the M^{n+}/M electrode prepared by the following procedure. Galvanostatic electrolysis was conducted at –50 mA cm^{-2} using a molybdenum electrode for 20 s, and then, the open-circuit potential was measured, as shown in Figure 2. The potential measured immediately after the electrolysis was the M^{n+}/M potential.

In the positive potential region of the cyclic voltammogram, the anodic current increased from about 3.40 V, as shown in Figure 3. Because chloride ions were the only anions in this melt, the anodic currents were considered to be due to the oxidation of chloride ions to chlorine gas.

$$2Cl^- \rightarrow Cl_2 + 2e^- \quad [1]$$

After the potential sweep direction was reversed (to negative), the current constantly decreased, eventually falling to zero at 3.46 V.

[z]E-mail: eum1901@mail4.doshisha.ac.jp

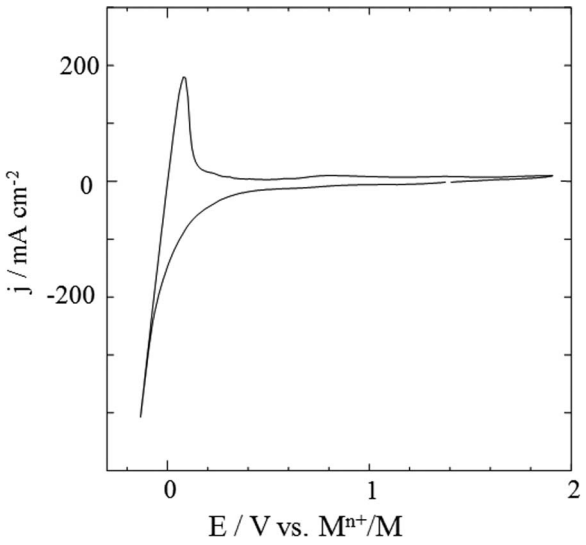

Figure 1. Cyclic voltammograms for a Mo electrode in $CaCl_2$-KCl at 923 K. Scanning rate: 0.1 Vs^{-1}.

This potential was defined as the potential of the anodic limit, since it is regarded as the Cl_2/Cl^- potential. From the CV results, the electrochemical window was determined to be 3.46 V.

Cyclic voltammetry.— In order to investigate the electrochemical behavior of the calcium ions, cyclic voltammetry was conducted in molten $CaCl_2$-KCl at 923 K. Figure 4 shows the cyclic voltammograms for a Si electrode at a scanning rate of 0.1 V s^{-1} at 923 K.

The electrochemical behavior of a Mo electrode was also investigated for comparison, because Mo does not form an alloy with Ca.[18] Figure 4 shows the typical cyclic voltammograms for Mo and Si electrodes at a scanning rate of 0.1 V s^{-1}. For the Mo electrode, a sharp increase in the cathodic current was observed at 0.2 V. Since Mo does not form alloys with Ca and K, the cathodic current was considered to be due to Ca or K metal deposition. After reversing the scanning direction at 0.10 V, a large anodic current peak was observed, because of the anodic dissolution of Ca or K metal.

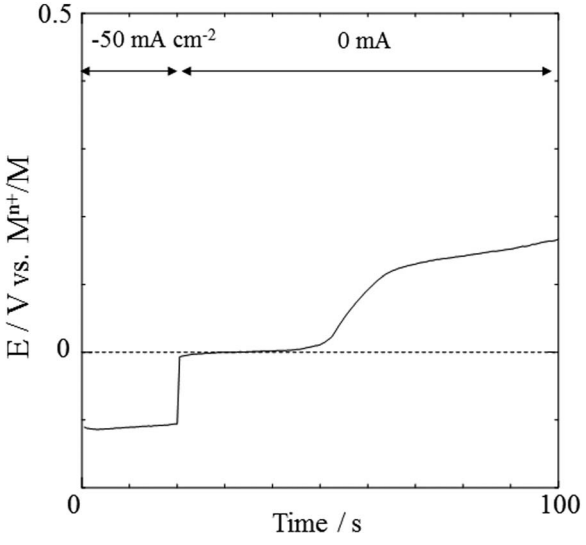

Figure 2. Open-circuit potential transient curve for the Mo electrode in the $CaCl_2$-KCl system at 923 K. Before the measurement, Ca metal was electrodeposited at the electrode by galvanostatic electrolysis at −50 mA cm^{-2} for 20 s.

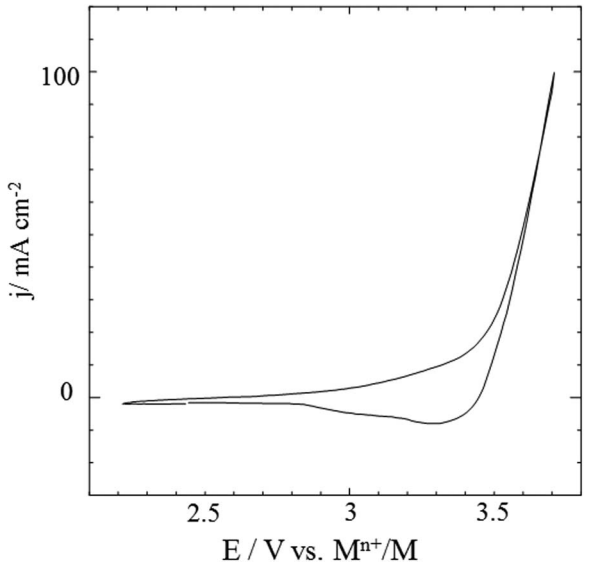

Figure 3. Cyclic voltammogram for a glassy carbon electrode in $CaCl_2$-KCl at 923 K. Scanning rate: 0.1 Vs^{-1}.

For the Si electrode, cathodic currents were observed from 1.20 V. Since this potential was more positive than the potential for Ca metal deposition, the cathodic currents were attributed to the formation of Ca-Si alloys. The standard formal potentials of Ca_2Si, CaSi, and $CaSi_2$ were 0.35, 0.46, and 0.49 V, respectively, as calculated from the corresponding standard Gibbs energies of formation.[19] These results agreed with those deduced from the cyclic voltammogram in Figure 4.

When the potential scan direction was reversed at −0.10 V, several anodic peaks were observed at 0.35, 0.65, and 1.00 V, respectively, indicating Ca dissolution from the different Ca-Si alloy phases.

Formation of Ca-Si alloy.— Based on the results of cyclic voltammetry, an alloy sample was prepared by potentiostatic electrolysis on a Si electrode at −0.10 V for 1 h. Figure 5 shows the XRD pattern of the sample. The spectrum showed peaks assignable to CaSi, $CaSi_2$, and the Si substrate, along with several unknown peaks.

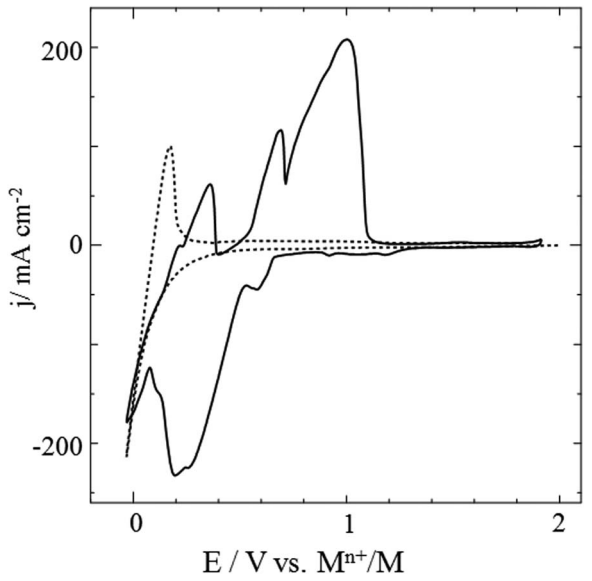

Figure 4. Cyclic voltammograms for Mo and Si electrode in $CaCl_2$-KCl at 923 K. Scanning rate: 0.1 V s^{-1}.

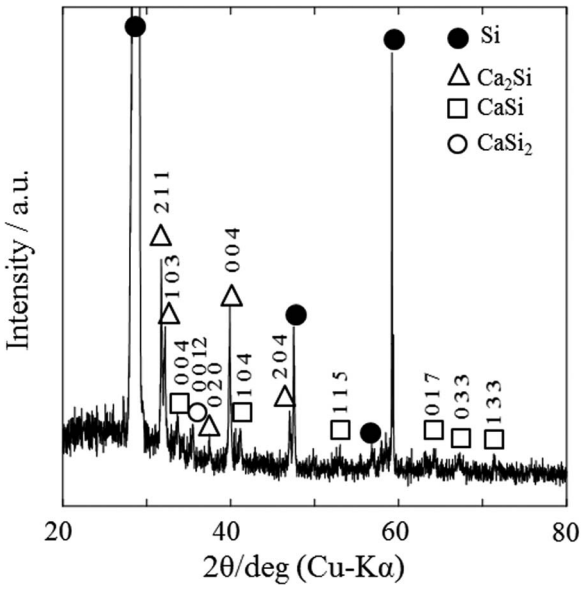

Figure 5. XRD pattern of the sample obtained by potentiostatic electrolysis with a Si electrode at −0.10 V for 1 h in $CaCl_2$-KCl eutectic at 923 K.

Figure 6 shows a cross-sectional SEM image of the sample and the concentration profiles of Ca and Si obtained by EDS line analysis. The observed alloy layer with a thickness of approximately 30 μm was considered to comprise CaSi and $CaSi_2$ layers, in accordance with the XRD result.

Phase control of Ca-Si.— The phase diagram of the Ca-Si system is shown in Figure 7.[18] According to this diagram, three Ca-Si intermetallic compounds having Ca concentrations lower than those of $CaSi_2$, CaSi, and Ca_2Si should exist at 923 K.

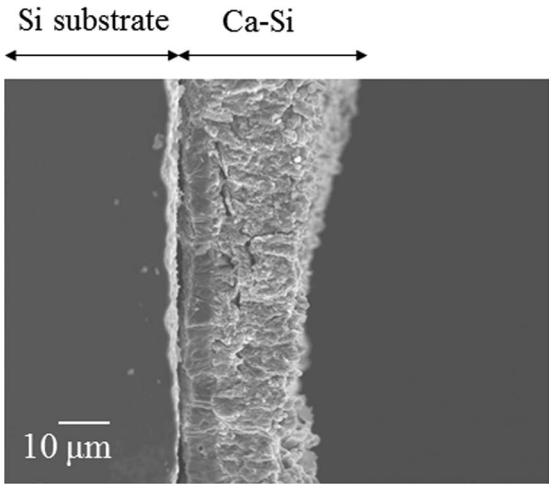

Figure 6. Cross-sectional SEM image and concentration profiles of Ca and Si for the sample at −0.10 V for 1 h.

Chronopotentiometry measurements were conducted to confirm the possibility of formation of Ca-Si alloy phases.

Open-circuit potentiometry was carried out to further investigate the formation of Ca-Si alloys. Figure 8 shows the open circuit potential transient curve for a Si electrode after the deposition of Ca metal by galvanostatic electrolysis at −50 mA cm^{-2} for 60 s, in molten $CaCl_2$-KCl at 923 K.

As can be seen in the chronopotentiogram, the potential remained at 0 V for the initial 10 s, probably because of the presence of the deposited Ca metal on the electrode. Subsequently, plateaus were observed at 0.18, 0.47, and 0.57 V, which were possibly due to different coexisting Ca-Si phases. Based on this result, samples were prepared by potentiostatic electrolysis.

First, potentiostatic electrolysis was conducted at −0.10 V for 30 min. Then, anodic dissolutions of Ca were conducted for 30 min

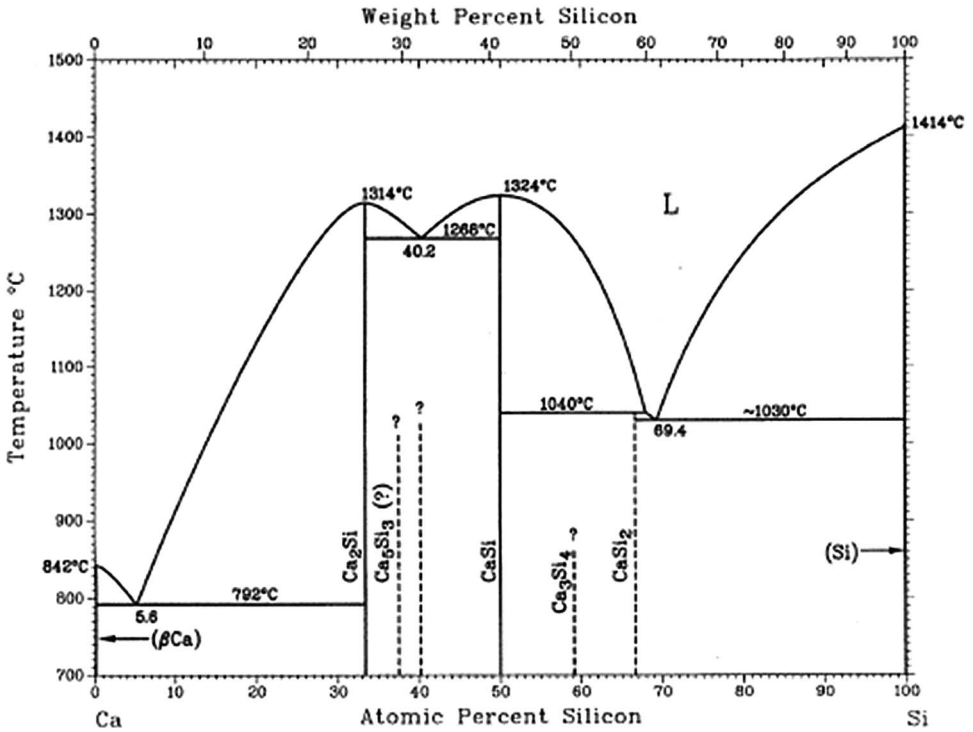

Figure 7. Phase diagram of the Ca-Si system.[18]

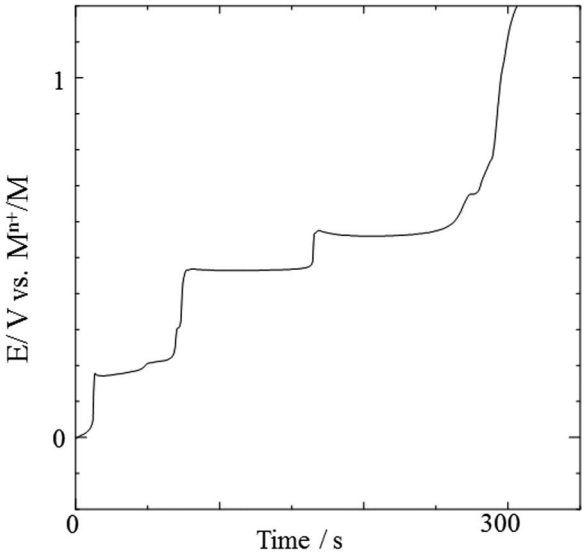

Figure 8. Open-circuit potential transient curve for the Si electrode in $CaCl_2$-KCl system at 923 K. Before the measurement, Ca metal was electrodeposited at the electrode by galvanostatic electrolysis at -50 mA cm^{-2} for 30 s.

by potentiostatic electrolysis at 0.10 (sample 1), 0.37 (sample 2), 0.50 (sample 3), and 0.78 V (sample 4). These potential values were determined by taking into account the potential plateaus before and after the potential jump indicating complete phase change.

The phases of the samples were analyzed by XRD, and the cross sections of the samples were observed by SEM.

Figure 9a shows the XRD pattern of sample 1 (obtained at 0.10 V). The alloy phase was identified as CaSi. Figure 9b shows the cross-sectional SEM of sample 1, indicating that the thickness of the CaSi film is about 10 μm. Figure 10a shows the XRD patterns of sample 2 (obtained at 0.37 V). The alloy phase was identified as $CaSi_2$. From the cross-sectional SEM image (Figure 10b), the thickness of the $CaSi_2$ film was determined to be about 20 μm.

Therefore, the potential plateau at 0.18 V was considered to correspond to the following reaction:

$$CaSi_2 + Ca\,(II) + 2e^- \Leftrightarrow 2CaSi \qquad [2]$$

Figure 11a shows the XRD pattern of sample 3 (obtained at 0.50 V), indicating Si and $CaSi_2$ phases. The cross-sectional SEM image in Figure 11b shows the film thickness to be about 20 μm. Figure 12a shows the XRD patterns of sample 4 (obtained at 0.78 V), revealing only Si peaks. Figure 12b shows the cross-sectional SEM image of sample 4, indicating that the transformed film is about 20 μm thick with a porous structure. Thus, the potential plateau at 0.57 V was considered to correspond to the following reaction:

$$2Si + Ca\,(II) + 2e^- \Leftrightarrow CaSi_2 \qquad [3]$$

These results suggested that phase control of the Ca-Si alloys is possible by appropriately adjusting the applied potential.

Optical properties of Ca-Si film.— The optical properties of the Ca-Si film, such as reflectance and absorption coefficient, were investigated as a function of wavelength by UV-VIS-NIR reflectance measurements. The reflection spectrum of the Ca-Si product in the

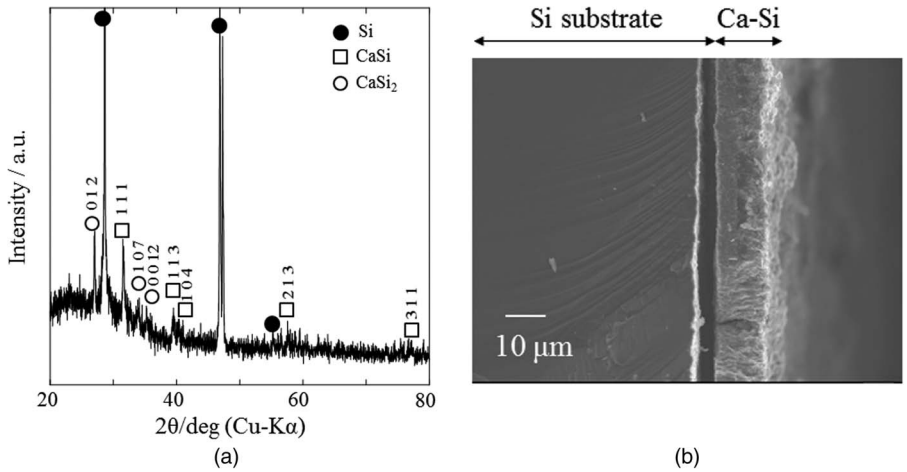

Figure 9. (a) XRD pattern of sample 1. (b) Cross-sectional SEM image of sample 1.

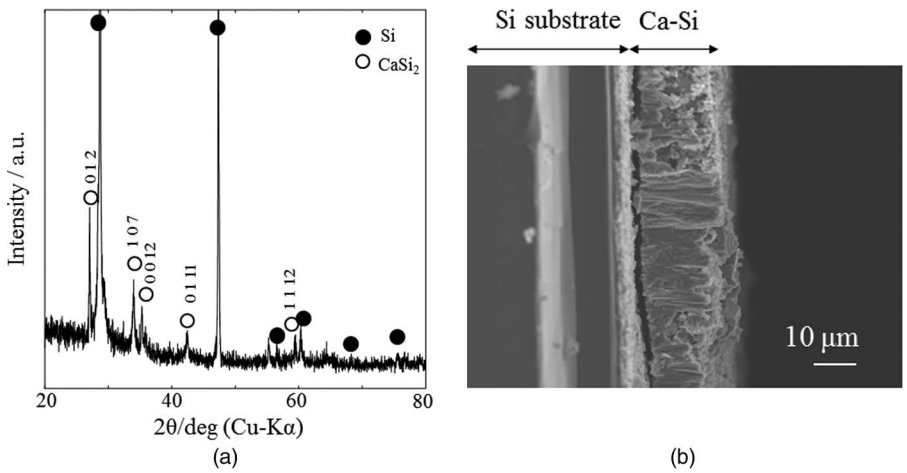

Figure 10. (a) XRD pattern of sample 2. (b) Cross-sectional SEM image of sample 2.

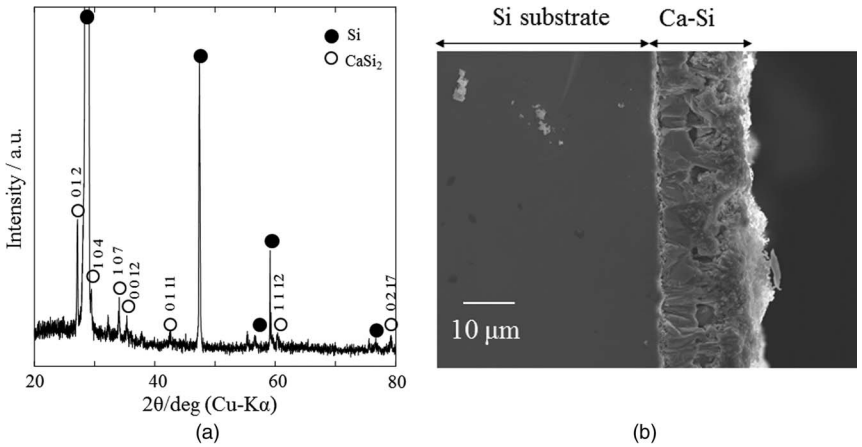

Figure 11. (a) XRD pattern of sample 3. (b) Cross-sectional SEM image of sample 3.

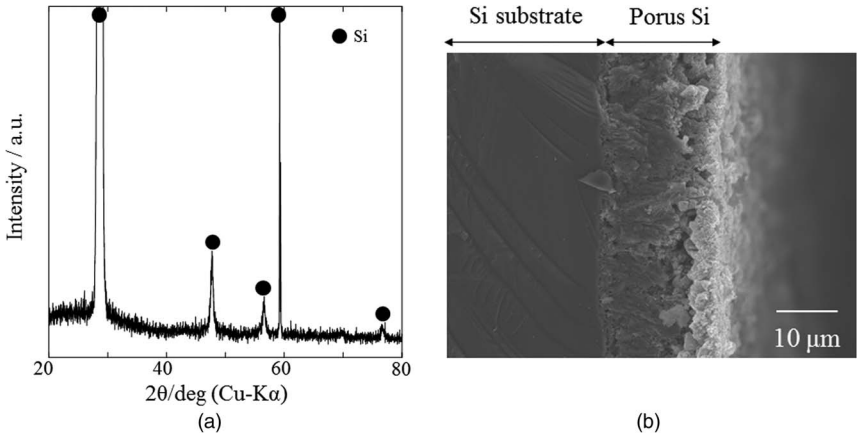

Figure 12. (a) XRD pattern of sample 4. (b) Cross-sectional SEM image of sample 4.

wavelength range 300–600 nm is shown in Figure 13, which reveals reflectance changes in the UV region. In the UV region, the Kubelka-Munk function[20,21] was used to convert the diffuse reflectance:

$$\alpha/S = (1 - R)^2/2R \quad [4]$$

where α is the absorption coefficient, S is the scattering coefficient, which is assumed to be constant and equal to 1, and R is the reflectance.

For determining the absorption edge of the semiconductors, the following equation applicable to a direct-band-gap semiconductor was used.

$$(h\nu\alpha)^2 = C\,(h\nu\text{-}Eg) \quad [5]$$

The band-gap energy was determined from the plot of $(h\nu\alpha/S)^2$ versus $h\nu$, which was linear, as illustrated in Figure 14. The band-gap value was obtained by extrapolating the straight portion of the graph on the $h\nu$ axis to $(h\nu\alpha)^2 = 0$, as indicated by the dotted line in the figure. Thus, the direct absorption edge was found to be located at 3.1 eV.

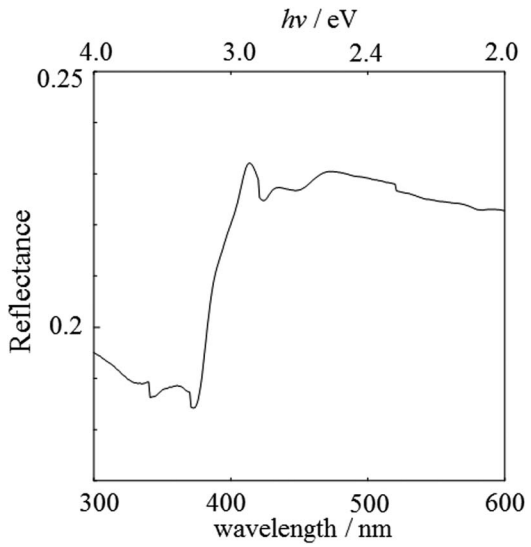

Figure 13. UV-VIS-NIR reflectance spectrum of sample 2.

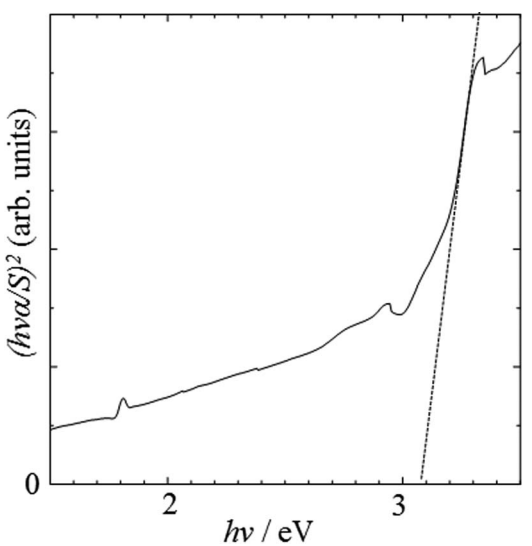

Figure 14. Absorption edge of sample 2.

From the present measurements, the bandgap of $CaSi_2$ was confirmed to be in the ultraviolet region.

Conclusions

The electrochemical formation of a Ca-Si alloy was investigated in $CaCl_2$-KCl at 923 K. The electrochemical window of $CaCl_2$-KCl was found to be 3.46 V at 923 K. Potentiostatic electrolysis of a Si electrode at −0.10 V resulted in the formation of a multiphase Ca-Si film having a thickness of about 30 μm. The multiphase Ca-Si film was converted into a CaSi, $CaSi_2$, or Si phase by anodic potentiostatic electrolysis depending on the potential. The various transformation reactions and the corresponding equilibrium potentials were clarified. UV-VIS-NIR reflectance measurements confirmed that the bandgap of $CaSi_2$ is 3.1 eV with a direct absorption edge.

References

1. H. Lange, *Phys. Stat. Sol. B*, **201**, 3 (1997).
2. M. Eizenberg and K. N. Tu, *J. Appl. Phys.*, **53**, 6885 (1982).
3. K. Lefki, P. Muret, N. Cherief, and C. Cinti, *J. Appl. Phys.*, **69**, 352 (1991).
4. J. F. Morar and M. Wittmer, *Phys. Rev., B* **37**, 2618 (1998).
5. Y. Imai, A. Watanabe, and M. Mukaida, *J. Alloy Comp.*, **358**, 257 (2003).
6. O. Madelung, *Semiconductors basic data*, 2nd ed., Springer, Berlin (1996).
7. M. Aoki, N. Ohba, T. Noritake, and S. Towata, *Appl. Phys. Lett.*, **85**, 387 (2004).
8. S. Sanfilippo, H. Elsinger, M. Nunez-Reguerio, and O. Laborde, *Phys. Rev., B* **61**, R3800 (2000).
9. G. Satta, G. Profeta, F. Bernadini, A. Continenza, and S. Massidda, *Phys. Rev. B*, **64**, 104507 (2001).
10. A. Netz, R. A. Huggins, and W. Weppner, *J. Power Sources.*, **119**, 95 (2003).
11. J Wolfenstine, *J. Power Sources.*, **124**, 241 (2003).
12. H. N. Acharya, S. K. Dutta, and H. D. Banerjee, *Sol. Ene. Mat.*, **3**, 441 (1980).
13. T. Koga, A. Bright, T. Suzuki, K. Shimada, H Tatsuoka, and H. Kuwabara, *Thin Sol. Films.*, **369**, 248 (2000).
14. M. Sugiyama and Y. Maeda, *Thin Sol. Films.*, **381**, 225 (2001).
15. T. Nakamura, T. Suematsu, K. Takakura, F. Hasegawa, A. Wakahara, and M. Imai, *Appl. Phys. Lett.*, **81**, 1032 (2002).
16. T. Hosono, Y. Matsuzawa, M. Kuramoto, Y. Momose, H. Tatsuoka, and H. Kuwabara, *Solid State Phenom.*, **93**, 447 (2003).
17. Iu. Kogut and M. C. Record, *Intermetallics.*, **32**, 184 (2013).
18. T. B. Massalski, *Binary Alloy Phase Diagrams*, Vol. 2, Editor, ASM International, p. 953 (1990).
19. F∗A∗C∗T, http://www.crct.polymtl.ca/reacweb.htm.
20. P. Kubelka and F. Munk, *Z. Tech. Phys.*, **12**, 593 (1931).
21. P. Kubelka, *J. Opt. Soc. Am.*, **38**, 448 (1948).